ACS APPLIED MATERIALS & INTERFACES

www.acsami.org

Research Article

Hiking down the Free Energy Landscape Using Sequential Solvent and Thermal Processing for Versatile Ordering of Block Copolymer Films

Kshitij Sharma, Aman Agrawal, Ali Masud, Sushil K. Satija, John F. Ankner, Jack F. Douglas,* and Alamgir Karim*

Cite This: *ACS Appl. Mater. Interfaces* 2023, 15, 21562−21574

Read Online

ACCESS | Metrics & More | Article Recommendations | Supporting Information

ABSTRACT: The kinetics and morphology of the ordering of block copolymer (BCP) films are highly dependent on the processing pathway, as the enthalpic and entropic forces driving the ordering processes can be quite different depending on process history. We may gain some understanding and control of this variability of BCP morphology with processing history through a consideration of the free energy landscape of the BCP material and a consideration of how the processing procedure moves the system through this energy landscape in a way that avoids having the system becoming trapped into well-defined metastable minima having a higher free energy than the target low free energy ordered structure. It is well known that standard thermal annealing (TA) of BCPs leads to structures corresponding to a well-defined stable free energy minimum; however, the BCP must be annealed for a very long time before the target low free energy structures can be achieved. Herein, we show that the same target low-energy structure can be achieved relatively quickly by subjecting as-cast films to an initial solvent annealing [direct immersion annealing (DIA) or solvent vapor annealing (SVA)] procedure, followed by a short period of TA. This process relies on lowering the activation energy barrier by reducing the glass-transition temperature through DIA (or SVA), followed by a multi-interface chain rearrangement through sequential TA. This energy landscape approach to ordering should be applicable to the process design for ordering many other complex materials.

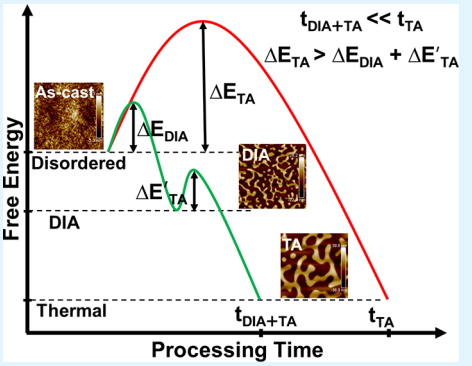

KEYWORDS: *block copolymer, thin film, self-assembly, thermal annealing, direct immersion annealing, solvent vapor annealing, neutron reflectivity*

INTRODUCTION

Block copolymers (BCPs) in the bulk exhibit many equilibrium morphologies[1,2] having similar free energies, and these materials are known to exhibit a tendency to become "stuck" in energetically metastable states having a morphology different from the equilibrium structure.[3−5] The inherent dynamic heterogeneity of glass-forming polymer materials on the scale of a few nanometers (nm) is another factor that tends to frustrate BCP ordering over large length scales.[6] Confinement of BCPs to thin films can be expected to add further frustration to ordering by altering the surface wetting of blocks and the order−disorder transition temperature[7−9] and thus, the overall stability of the ordered BCP morphology and often even the symmetries of the ordered phases. As a result, there are different morphologies that arise near the boundaries of thin BCP films.[10−12] For example, in the case of lamellar BCP films, where the lamellae are oriented parallel to the substrate due to preferential segregation of one block to the substrate/air interface,[13] the necessity of BCP films to be composed of an integral number of layers causes frustration at the free boundary, resulting in an incomplete boundary layer (island/hole topography) when the film thickness is not an integral multiple of the bulk lamellar domain size.[10,12] Finally, we mention that the introduction of nanoparticles exhibiting a tendency to associate, such as fullerenes, with BCP materials can lead to complete suppression of the BCP order−disorder transition.[14] In this case, the nano-filled BCP material instead is so frustrated that it forms a kind of metastable BCP glass in which the ordering at low temperatures is only local. For nano-filled homopolymer thin films, this frustration toward relaxation has been reported to enhance the film stability by suppressing dewetting.[15−17] In the present work, we are concerned with developing a conceptual framework and a corresponding experimental methodology to avoid trapping the material in undesirable metastable states and instead drive

Received: December 5, 2022
Accepted: April 10, 2023
Published: April 21, 2023

https://doi.org/10.1021/acsami.2c21924
ACS Appl. Mater. Interfaces 2023, 15, 21562−21574

it to the targeted desirable states for applications such as parallel lamellar capacitors[18,19] in a fashion that is relatively facile to implement.

Modi et al. and Longanecker et al. demonstrated using a solvent mixture immersion method termed direct immersion annealing (DIA) to overcome the kinetic hurdles faced by other annealing techniques to produce sharp domain interfaces.[20,21] DIA rapidly produces nanostructures with reduced domain sizes and narrower interfacial widths for symmetric (lamellar) BCP films. This process occurs in solution at room temperature and is useful for polymers with a high molecular mass and, therefore, low mobility, or for polymers that may degrade or crystallize at high temperatures, or even multicomponent systems like BCP nanocomposites. This method utilizes a combination of solvents that modulate the solubility of the solution to allow the polymer chains to rearrange while preventing dewetting and dissolution of the film. Modi et al. showed that there is a practical upper limit for the amount of good solvent in the solvent mixture which was found where the solubility parameter of the mixture reached a value close to that for PS, the majority block of the PS-*b*-PMMA studied. The solvent mixture optimization was mostly based on PS because PMMA adsorbs onto the SiO_x substrate. They also showed that the parallel domain orientation in DIA-annealed cylindrical (cyl) BCP films is related to the immersion time t as $\xi(t) = A_T\, t^n$, where ξ is the orientational correlation length, T is the absolute temperature, and n is the power law exponent. A_T is a T-dependent coefficient expressed as $A_T = \xi_{0,T}/t_0^n$, which is a prefactor that measures how fast the early-stage morphology develops. $\xi_{0,T}$ is the initial correlation length at time t_0 and temperature T.[22] Berry et al. found that this prefactor for a cyl-poly(styrene-*b*-methyl methacrylate) (PS-*b*-PMMA) film with a thickness of 170 nm thermally annealed at 180 °C is 15.48, while the same prefactor for DIA at 56 °C is (122 ± 23), where the uncertainty corresponds to one standard deviation.[23] The DIA prefactor was close to that found for a cyl PS-*b*-PMMA film of thickness 170 nm, A_T = (116 ± 10) (uncertainty represents one standard deviation), on annealing at 240 °C by Yager and Majewski.[24] A_T values obtained for DIA at different solvent mixture temperatures were fitted to an Arrhenius equation to obtain the activation energy for DIA and was found to be (111 ± 63) kJ/mol (this uncertainty value from ref 20 corresponds to one standard deviation). In comparison, Ruiz et al. reported a defect diffusion activation energy for a cylinder forming PS-*b*-PMMA with a number average molecular mass (M_n) of 64 kg/mol (64k) thin-film melts to be 270 kJ/mol.[22]

The DIA solvent combination is a mixture of a majority non-solvent and a polymer swelling solvent(s) to obtain a finely tuned chemical potential for BCP ordering without BCP film dissolution into the solvent mixture reservoir. As the polymers are fully submerged in the solvent, rapid ordering can occur compared to solvent vapor annealing (SVA), i.e., the chemical potential for BCP ordering is higher in DIA (direct contact with a high-density liquid phase) compared to SVA (direct contact with a low-density vapor phase). Furthermore, depending on the volume of the vapor phase environment, vapor phase equilibration times can be very variable, and the method requires precise controls. The enhanced mobility in the solvent-swollen BCP film (lowered T_g) accelerates segregation into domains, while the solvent quality alters the Flory Huggins interaction parameter (χ) that modifies the interfacial width. If the solvent mixture is neutral and good for both blocks, the interaction parameter between the blocks is effectively reduced. On the other hand, in the presence of a block selective solvent(s) component, the effective interaction parameter may be enhanced, which reduces the interfacial width. This insight was used to reversibly homogenize and phase separate binary mixtures of polymer-grafted nanoparticle brush thin films simply by changing the solvent(s) composition.[25] Zeman and Patterson predicted this increment in χ to be proportional to the square of the difference between individual interaction parameters for blocks 1 and 2, and the selective solvent s, as shown below[26]

$$\chi_{12} \approx \frac{(\chi_{1s} - \chi_{2s})^2}{(\delta_1 + \delta_2 - 2\delta_s)^2}\frac{RT}{\nu} \quad (1)$$

Here, R is the universal gas constant, T is the absolute temperature, δ is the solubility parameter, and ν is the molar volume. Longanecker et al. reported $\chi_{\text{PS-acetone}}$ and $\chi_{\text{PMMA-acetone}}$ to be 0.9 and 0.48, respectively,[21] making acetone selective to one block (PMMA), which leads to an effective interaction parameter value of $\chi_{\text{PS-PMMA}}$ = 0.59. The actual interaction parameter is lower than 0.59 due to the presence of heptane (non-solvent) and toluene (neutral good solvent). Based on the concentration of the good solvent, the solubility and, therefore, the swelling ratio of the film may be modulated to control the segregation/deposition rate. The ability to control chain mobility may help us explore morphologies stable only under certain chemical potential fields. Sinturel et al. summarized BCP morphology evolution for SVA with different solvent mixtures and annealing conditions and reported that the nature of the solvent vapor mixture could have a significant impact on the film microstructure.[27] One such metastable state/microstructure can also be obtained on fast solvent evaporation after removing the film from the DIA solution. The rapid drying shrinks the swollen parallel lamellar domains without allowing chains to rearrange, producing a microstructure with reduced domain sizes (up to ≈50% lower) and a greater number of unlike interfaces (up to ≈50% higher). The rapid evaporation of the solvent from a swollen film prevents the rearrangement of chains to their natural junction spacing (J_2) at the interfaces observed after TA. The DIA microstructure gets stuck with the higher J_1 of the solvent-swollen film, and the lamellar layers then take up a collapsed brush structure to fill the space left behind by the evaporating solvent.

In view of the qualitative analogy of frustrated mesoscale ordering processes in BCP materials and glass-formation in molecular liquids, it is useful to draw upon a methodology developed in the field of glass-forming materials to "chaperone" the system into a target functional state in a way that is both economical and which does not require a great deal of time and effort. We note that nature addresses this problem in the context of the ordering of proteins into their functional globular state through the confinement of the proteins inside chaperone complexes that modulate accessible protein conformations and limit the accessible free energy landscape; recent work has been aimed at synthetically emulating this process.[28]

Recently, it was found that films of small molecules can be formed in exceptionally low potential energy states through chemical vapor deposition.[29,30] While it is normally quite difficult to volatilize polymers, we can simulate vapor-state deposition by simply dissolving the polymer in a solvent and

https://doi.org/10.1021/acsami.2c21924
ACS Appl. Mater. Interfaces 2023, 15, 21562−21574

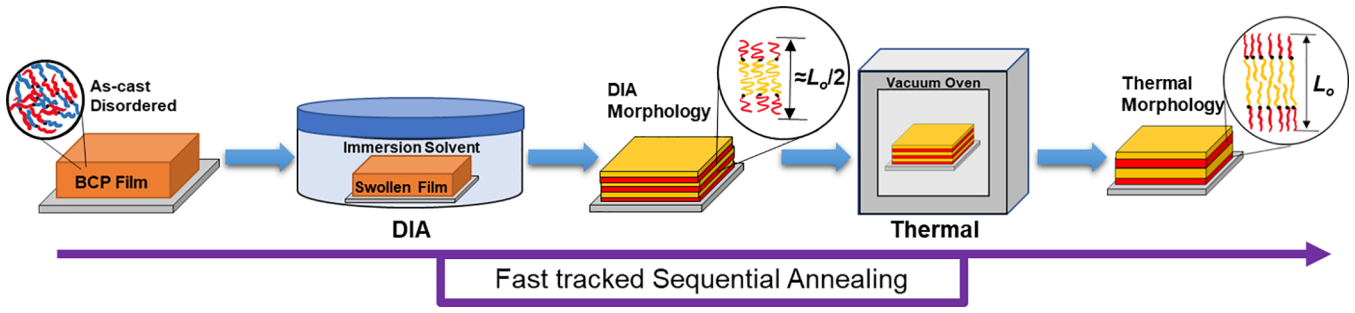

Figure 1. Sequential annealing methodology by sequential DIA and TA.

treating this solution phase deposition as an analogue of chemical vaporization that is appropriate for polymer materials. We explore this methodology to create BCP films whose properties are engineered by controlling the film deposition process. The high interfacial mobility of the deposited film in chemical vapor deposition is thought to be the key physical factor in lowering kinetic barriers to achieve a low energy state of the material. We may expect this feature to also arise in an appropriately designed solution phase process for polymers. The solution process has the added feature that, in addition to reducing the kinetic barriers, it is also possible to engineer the thermodynamic driving force for the ordering process through the appropriate choice of the solvent, e.g., the bulk and interfacial χ parameters of BCPs. The solvent normally plasticizes the segmental polymer dynamics, lowering T_g and reducing the dynamic heterogeneity effect mentioned above in a way similar to subjecting the BCP films to a transient heat treatment.[23,31] We expect the solution deposition method to be useful in the formation of materials composed of complex molecules exhibiting complex interactions, which tend toward polymorphic ordering into thermodynamic states having similar energies, as epitomized by BCP materials.

We find that solvent processing of BCP films enables us to probe energy states that we could not readily access by simply thermal annealing (TA) flow-cast/spin-cast films of the same BCP materials for any reasonable time. The solvent processing methodology achieves a metastable energy state after a relatively short time, and the method is facile. Using a combinatorial method allows us to avoid getting stuck and traverse through the metastable states toward the global energy minimum. We also find that ordering occurs analogously to Ostwald's "Rule of Stages", in which the BCP material evolves through a series of well-defined metastable stages, and that we can prepare BCP polymer films to map the metastable states having very different morphologies through control of immersion conditions.[32,33] Metastable states are common in polymer materials. In the instance of lamellar BCPs, the lamellar thickness in the metastable and equilibrium states can differ by a factor of up to two that scales with molecular mass, reminiscent of the transition between unfolded and folded alkane crystals.[34,35] We anticipate that both metastable and minimal free energy structures may find useful applications, and the ability to engineer such structures will aid in material design.

Combinatorial annealing methods were previously reported for targeted and accelerated BCP assembly in thin films. An up-and-coming candidate is the solvothermal annealing process which enhances molecular motions in solvent vapor swollen films at elevated temperatures. Gotrik and Ross reported a two-stage solvothermal method for a cylinder forming high-χ poly(styrene-*b*-dimethyl siloxane) (PS-*b*-PDMS) copolymer, where the effect of solvent vapor uptake and film heating processes were decoupled.[36] Zhang et al. demonstrated the use of a combined microwave-SVA technique for poly(styrene-*b*-2-vinyl pyridine) (PS-*b*-P2VP) and poly(styrene-*b*-methyl methacrylate) (PS-*b*-PMMA) BCPs, where the elevated temperatures were obtained from microwave excitation of neat and patterned Si substrates.[37] Process parameters include the solvent environment, temperature, and substrate resistivity and chemistry that can be optimized to obtain BCP morphologies with low defect densities over significantly shorter annealing durations. Parallel thermal and SVA annealing was proposed by Cummins et al., where elevated temperatures increased the vapor pressure, in turn increasing the density of vapor inside the swollen film.[38] This enhanced molecular diffusion by lowering the glass-transition temperature of the system. Shi et al. demonstrated a two-step annealing process that combined SVA and TA treatments to obtain enhanced vertical lamellar assembly from a cylindrical rod-coil diblock of poly (dimethylsiloxane)-*b*-poly{2,5-bis[(4-methoxyphenyl)-oxycarbonyl]styrene}, a high χ BCP.[39] The study did not, however, focus on the kinetic and mechanistic details of the sequential assembly processes.

Longanecker et al. discussed lamellar BCP films of low M_n (32.5k) PS-*b*-PMMA to obtain thermally annealed domain size, L_o (standard domain size terminology for melt annealed films), from a DIA-annealed morphology via successive thermal treatments.[21] They extended the process to nano-filled BCP films and demonstrated enhanced and accelerated self-assembly via DIA. This study did not explore the reversible transition between the two ordered states or how this transformation differs from ordering from a disordered state, nor the possibility of finding an alternate processing route to overcome slow diffusion and non-equilibrium (metastable) morphologies. Compared to the direct transition to a thermal equilibrium morphology, the sequential study will help us understand and develop transition pathways for enhanced BCP assembly by integrating DIA (or SVA) and TA pathways in a serial manner via a study of individually controlled process times (t) on the final ordered state, i.e., DIA (t_{DIA}) + TA (t_{TA}). In this work, we report accelerated BCP self-assembly with large L_o (as opposed to the $\approx L_o/2$ obtained by DIA alone) by combining these techniques that replace the single large energetic barrier toward self-assembly observed in BCP melts with two cascading steps having a smaller overall barrier (methodology described in Figure 1). While lower molecular mass polymers are easy to process with conventional techniques, this alternate energy pathway shows promise to improve the processibility of high molecular mass BCPs. Tracking the transitions for these large molecular mass systems

https://doi.org/10.1021/acsami.2c21924
ACS Appl. Mater. Interfaces 2023, 15, 21562−21574

with slow kinetics allowed us to study mechanisms for domain restructuring. We did this by systematically observing transitions for a series of molecular masses (below and above entanglement) of lamellar PS-*b*-PMMA BCPs using atomic force microscopy (AFM) to measure the surface topography of the island/hole morphology in incommensurate films and neutron reflectivity (NR) to probe the internal film restructuring.

RESULTS

Equilibrium and Metastable Lamellar Morphologies.

Achieving highly ordered lamellar assembly for large molecular mass BCP (typically $M_n \geq$ 40k-*b*-40k) thin films has not been feasible using conventional polymer processing techniques. While TA of high M_n BCPs is slow, faster processing techniques like SVA and the more recent DIA produce non-equilibrium morphologies with significantly reduced domain size. Also, knowledge regarding the stability of the trapped metastable morphology is very limited in techniques like DIA. In this paper, our research aims to explore and understand film ordering kinetics, morphology evolution, molecular diffusion mechanisms, and the energetics of transition between ordered states produced by sequential DIA and TA. We accomplish this using thin BCP films cast via the flow coating method, with thicknesses ranging from 120 to 180 nm and different molecular masses. The variability in film thickness is to make sure that there are multiple lamellae formed for any BCP molecular mass studied. We anneal the films sequentially from as-cast to DIA (or SVA) to TA. Due to an oxide layer on the ultraviolet ozone (UVO)-treated substrates, the film's internal lamellar morphology for annealed symmetric (sym) PS-*b*-PMMA is parallel to the substrate. This alignment is confirmed by the observation of island/hole surface morphology using AFM, characteristic of incommensurate film thicknesses. All AFM measurements were performed in incommensurate regions of the annealed films.

Parallel lamellar morphology was also confirmed with NR for the deuterated symmetric BCP (dPS-*b*-PMMA) with overall M_n = 62k. This BCP has a deuterated PS block and is the closest commercially available polymer compared to the molecular mass of the primary BCP studied via AFM (66k). At this molecular mass, the first and second-order Bragg peak positions were seen at wave vector values (Q) of 0.23 and 0.38 Å^{-1}, respectively, for a thermally annealed film. The same peaks for a DIA-annealed film were observed at 0.34 and 0.63 Å^{-1}. The positions have been extracted from the processed NR data. The domain size (L_o) can be evaluated from the through-plane height of islands/holes in the AFM height scans[40,41] or via Bragg peak locations in the NR data. The Q^* values in the figures show the primary Bragg peak position, which is inversely proportional to the domain size. Longanecker et al. studied lamellar dPS-*b*-PMMA (19.5k-*b*-18.1k) via NR to obtain L_o equal to 25.9 nm ($L_{o,TA}$) for thermal and 14.7 nm ($L_{o,DIA}$) for DIA processed films.[21] These domain sizes for both TA and DIA are stable at long time scales, and these values for the currently studied set of BCPs were estimated via island/hole height measurements from AFM height sensor scans and are listed in Table 1. The through-plane height of the island/hole features for an incommensurate film thickness corresponds to the domain size (L_o) of the BCP for a particular treatment method.[40−42] These control measurements provided us with the domain sizes for parallel lamellae obtained using the two annealing techniques at their respective equilibrium states from a disordered as-cast state. The time needed for TA to achieve equilibrium assembly ranged from 24 h for M_n = 36.5k (19.5k-*b*-17k), 51k (25k-*b*-26k), and 66k (33k-*b*-33k) at 180 °C to 48 h for M_n = 89k (45k-*b*-44k) at 200 °C. The increased treatment times and temperatures are required due to reduced molecular diffusivity with increasing chain length N, as per the Rouse approximation.[22] The order−disorder temperatures (T_{ODT}) for this BCP were reported by Ahn et al. for M_n = 29.2k and M_n = 35.6k to be 200 and 250 °C, respectively, and they showed that the T_{ODT} increased with increasing molecular mass.[43] The annealing temperatures used for this work are all below the T_{ODT} for any PS-*b*-PMMA molecular mass used. To achieve equilibrium assembly, the DIA treatment time ranged from 1 h for M_n = 36.5k to 66k in solvent mixture 1 (SM_1) to 3 h for M_n = 89k in SM_2. DIA for BCP with M_n = 89k in SM_1 may take up to 12 h. We further show in Figure S1 of the Supporting Information that SM_2 was substantially more time efficient in the DIA ordering step (3 h in SM_2 vs 24 h in SM_1) for a sym BCP with higher M_n = 132k (65k-*b*-67k). TA requirements for BCP with M_n = 132k are 48 h at 220 °C. Again, as diffusion slows down with increased molecular mass, a solvent mixture with a higher solubility parameter (SM_2) is necessary to achieve fast assembly. At the other extreme, for very low molecular mass BCPs like that with M_n = 20k (10k-*b*-10k), DIA in SM_1 dewets the thin film, and a solvent mixture with lower solubility (SM_0) can order this BCP. A long-time TA treatment at 180 °C for a film of this BCP cannot produce the island/hole topography. Figure S2 shows AFM and optical microscopy images for PS-*b*-PMMA (M_n = 20k) film annealed via TA at 180 °C and DIA in SM_1 and SM_0, highlighting how the DIA solvent mixture can be tuned for efficient self-assembly of BCPs with different molecular masses. As reported previously,[21] TA produced parallel domains with a much larger size (L_o) than those produced by DIA (≈0.3L_o to 0.5L_o, also observed for all our DIA solvent mixture processed films, i.e., SM_1 and SM_2). The present study analyzes the enhanced ordering kinetics and structural rearrangement mechanisms for the sequential DIA (or SVA) to TA annealing process compared to traditional TA alone.

Additionally, the effects of SVA in various common solvents were studied for PS-*b*-PMMA with M_n = 51k and 66k, both for SVA-alone and SVA + TA sequential annealing. SVA was performed at room temperature in sealed jars with a solvent bath volume of ≈5 mL. The solvents used included pure acetone (selective toward PMMA), pure tetrahydrofuran (THF—good solvent for PS and PMMA), and mixtures of heptane, acetone, and toluene (SM_1). Films annealed via SVA in acetone quickly developed island/hole surface topography (5 to 15 min), representative of a parallel lamellar morphology.

Table 1. Polystyrene-*b*-poly(methyl methacrylate) BCPs Molecular Mass Studied and Associated Microstructure Lamellar Domain Sizes[a]

PS-*b*-PMMA M_n (kg/mole)	thermal $L_{o,TA}$ (nm)	DIA $L_{o,DIA}$ (nm), SM_n[b]
36.5 (19-*b*-17.5)	21	14, SM_1
51 (25-*b*-26)	28	19, SM_1
62 (29.5-*b*-32.5)[a]	37	25, SM_1
66 (33-*b*-33)	36	27, SM_1
89 (45-*b*-44)	45	33, SM_2
132 (65-*b*-67)	58	38, SM_2

[a]Deuterated PS. [b]SM_n - solvent mixture used for DIA.

https://doi.org/10.1021/acsami.2c21924
ACS Appl. Mater. Interfaces 2023, 15, 21562−21574

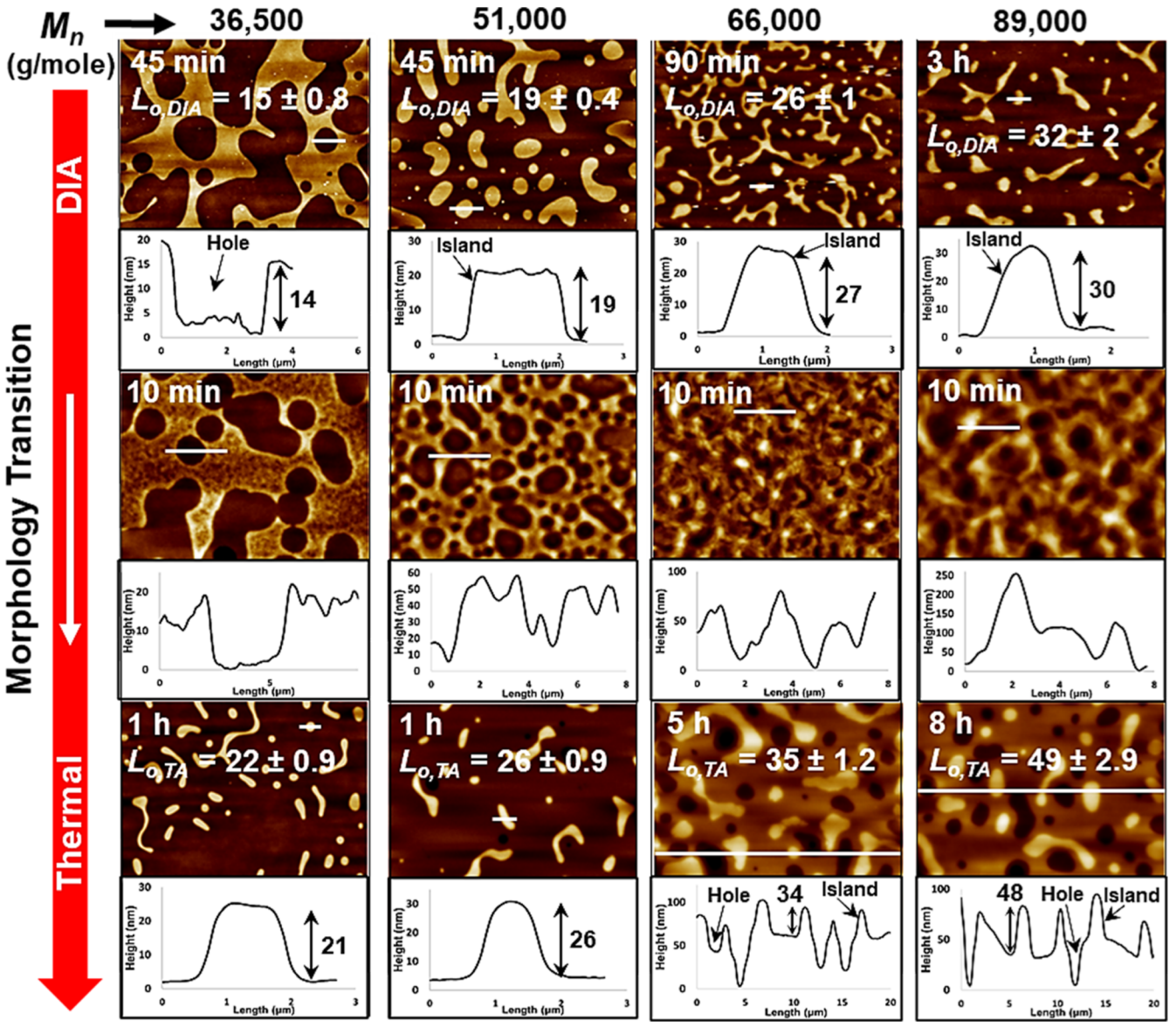

Figure 2. AFM height sensor images and line height profiles showing topographical data for row 1: PS-*b*-PMMA films annealed via DIA in SM_1 (columns 1 to 3: M_n = 36.5k, 51k, and 66k) and SM_2 (column 4: M_n = 89k); row 2: DIA-annealed films from Row 1 successively annealed thermally at 160 °C (M_n = 36.5k, 51k, and 66k) and 180 °C (M_n = 89k) showing the undulating transition state for this route; row 3: DIA-annealed films from row 1 sequentially annealed thermally at 180 °C (M_n = 36.5k, 51k, and 66k) and 200 °C (M_n = 89k) showing transition to the thermal microstructure of large island/holes. AFM images for M_n = 36.5k and 51k show a complete transition to single-layered island/holes with a large height. AFM image for M_n = 66k has 3 terraces, and for M_n = 89k has 2 terraces due to multilayered chain rearrangement. L_o values in the inset are average island/hole heights, and the error is the standard deviation for multiple measurements on the image. We distinguish between the two domain sizes using subscripts, and so, $L_{o,TA}$ for the TA domain size, and $L_{o,DIA}$ for the DIA domain size. Annealing times are in the inset top left, and numerical in the line height profile images are island/hole heights in nm obtained by AFM for the features marked by white horizontal lines in the images.

The feature heights were calculated from AFM height sensor images, and the average $L_{o,SVA}$ was found to be 16 nm for BCP with M_n = 66k. This is much smaller than the average $L_{o,TA}$ (≈55% smaller) and also lower than $L_{o,DIA}$ (≈40% smaller). The lamellar layers are evidently very thin so that the microstructure is a non-equilibrium state. Films annealed for extended durations (up to 3 h) also developed shrunken domains of domain size ≈ 16 nm. The domain sizes were found to be smaller than those for DIA in SM_1 because film swelling in the presence of pure acetone vapor may be expected to be higher compared to the solvent mixture that has a majority of bad solvent. When acetone was replaced by THF, the films did not produce any island/hole topography. High-resolution AFM scans (1 μm × 1 μm) revealed a poorly ordered vertical lamellar assembly instead, for the treatment durations studied (up to 4 h). Figures S3 and S4 show AFM scans for PS-*b*-PMMA (66k) annealed in acetone and THF vapors, respectively. In addition to using pure solvents, solvent mixtures with a majority portion of a bad solvent (heptane) were also tested for SVA of PS-*b*-PMMA with M_n = 51k and 66k. The SM_1 composition was used for SVA for 2 h which ordered films of both molecular masses into a parallel lamellar morphology. Figure S5 shows AFM height sensor images for the BCP films, where the domain sizes for both the BCPs were

https://doi.org/10.1021/acsami.2c21924
ACS Appl. Mater. Interfaces 2023, 15, 21562−21574

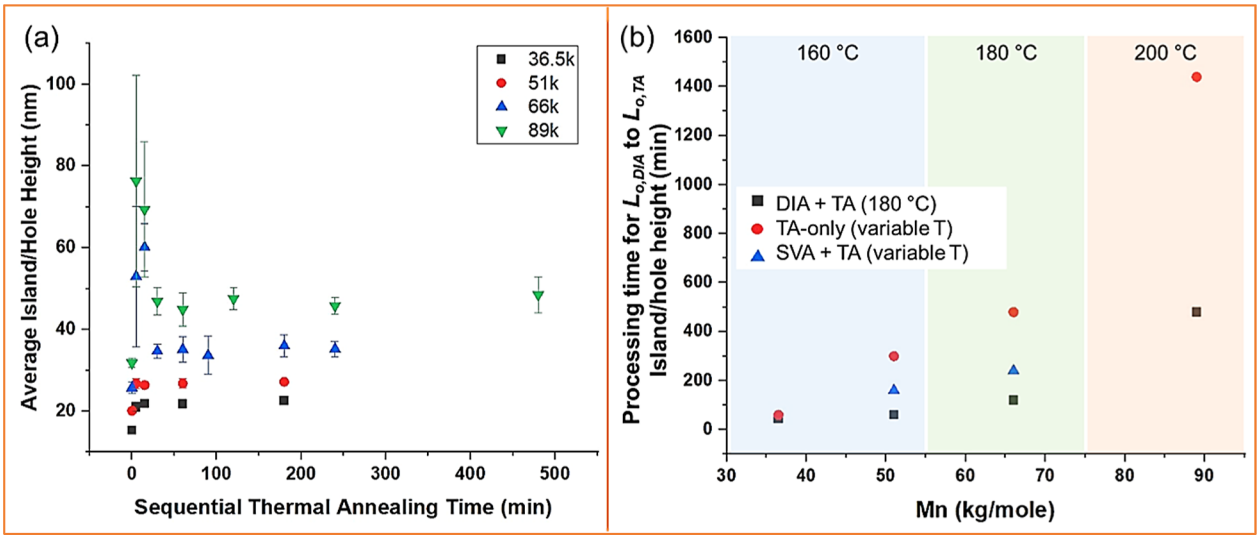

Figure 3. (a) Average island/hole size (perpendicular to the film surface) from AFM height sensor analysis plotted against sequential TA time. Sizes increase from the DIA-annealed domain size at time zero to approximately the thermally annealed domain period in a very short time. (b) Time of transition from DIA ($\approx L_o/2$) to thermal (L_o) morphology tracked via AFM vs BCP molecular mass. The exponent for M_n was fitted to ≈0.055, and the uncertainty in the fit corresponds to a reduced chi-squared value of 777.0 for the optimal fit to the data. (b) also shows TA-only times for all molecular masses studied and sequential SVA+TA annealing times for M_n = 51k and 66k.

obtained from island/hole height measurements and observed to be lower than their respective TA domain sizes. For BCP with M_n = 51k, island/hole topography was observed to develop within 1 h of SVA. On the other hand, the BCP with higher molecular mass-produced poor order compared to the lower M_n studied and needed extended SVA to develop a regular island/hole morphology corresponding to the SVA domain size (see Figure S5e). The SVA periodicity for annealing in SM_1 closely matches to that observed for DIA. By comparison, we have shown that DIA in the same SM_1 can order BCP with M_n = 66k in ≈1 h. For the BCP molecular mass studied here, DIA is ≈2+ times faster than SVA.

Sequential Annealing Using Solvent and Thermal Processes. A PS-*b*-PMMA molecular mass series (M_n = 36.5k to 89k) was tested for the transition from a DIA-annealed microstructure ($\approx L_o/2$) to a TA-processed microstructure (L_o). Figure 1 schematically shows the sequential annealing process used where domain size terminologies of $L_{o,DIA}$ and $L_{o,TA}$ are used to clearly distinguish between DIA and TA domain sizes, respectively. AFM analysis reveals a smaller island/hole height for the DIA-treated film. In addition to hot stage drying, a set of film samples (M_n = 66k) were vacuum (≈100 kPa) dried at 80 °C for 24 h to study the effects of residual solvent, if any, left behind after the first DIA step. These DIA-annealed films were then annealed thermally (TA) at 180 °C (M_n = 36.5k to 66k) and 200 °C (M_n = 89k) in a vacuum for 24 h. AFM measurements on the resulting films revealed a transition to the standard thermally annealed L_o for both stage dried at 60 °C (our standard drying procedure) and vacuum oven dried films, with nearly similar transition kinetics (transition time from $\approx L_o/2$ to L_o). Thus, we conclude that residual solvent, if any, after our standard hot stage drying, for which the bulk of our DIA + TA data is reported, does not play a role in the transitions. The film thickness before and after DIA and further after the TA treatment were observed to be the same, indicating that the change in island/hole heights is a consequence of lamellar domain restructuring. To study the kinetics of the transition, DIA-equilibrated films were thermally annealed at the same temperatures for shorter durations to achieve partially re-ordered metastates, i.e., different metastable transition states en route to the subsequent TA microstructure. AFM scans of the surface topography of these films are shown in Figure 2. It was observed that after as little as 15 min TA at 180 °C ($T \gg T_{gBCP}$), the surface morphology changed and island/hole height increased. Subsequent TA slowly refined this microstructure to produce a fully developed island/hole topography (L_o) with sharp domain boundaries over the next few hours. Lower molecular mass (M_n = 36.5k and 51k) BCP films displayed a swift (1 h) transition to a refined microstructure at 180 °C with larger TA domains. In contrast, higher molecular mass polymers (M_n = 66k and 89k) needed longer sequential TA time (5 to 10 h) to achieve well-developed larger TA domains. The island/hole heights measured by AFM, tracked from the starting DIA-annealed state into the subsequent thermally annealed island/hole heights at 180 °C (black squares), are plotted in Figure 3 and show exponential growth for the times required for transition with increasing BCP molecular mass. These "transition times" are the sequential TA times for the island/hole heights to increase from the DIA ($\approx L_o/2$) domain size to that for TA (L_o).[44] The figure also shows annealing times for TA-only treatment (red circles) at 160 °C for M_n = 36.5k and 51k, at 180 °C for 66k, and at 200 °C for 89k BCP. Additionally, Figure 3 also shows SVA + TA time for the transition in island/hole heights from SVA-ordered morphology in SM_1, followed by TA at 160 °C for M_n = 51k and at 180 °C for 66k (blue triangles). Both the DIA + TA times and SVA + TA processing times are lower than TA-only times, especially for the largest molecular mass BCP studied. We use this convenient AFM methodology to identify the annealing time wherein the internal ordering is fully complete [Masud et al. have confirmed this with AFM and NR].[42] Notably, the combined annealing time (t_{DIA+TA}) is much shorter than the traditional TA-only time (t_{TA} = 24 to 48 h).[45] The combination of DIA and TA thus provides a route to achieve "fast-track" ordering of BCP into a similar parallel lamellar

https://doi.org/10.1021/acsami.2c21924
ACS Appl. Mater. Interfaces 2023, 15, 21562−21574

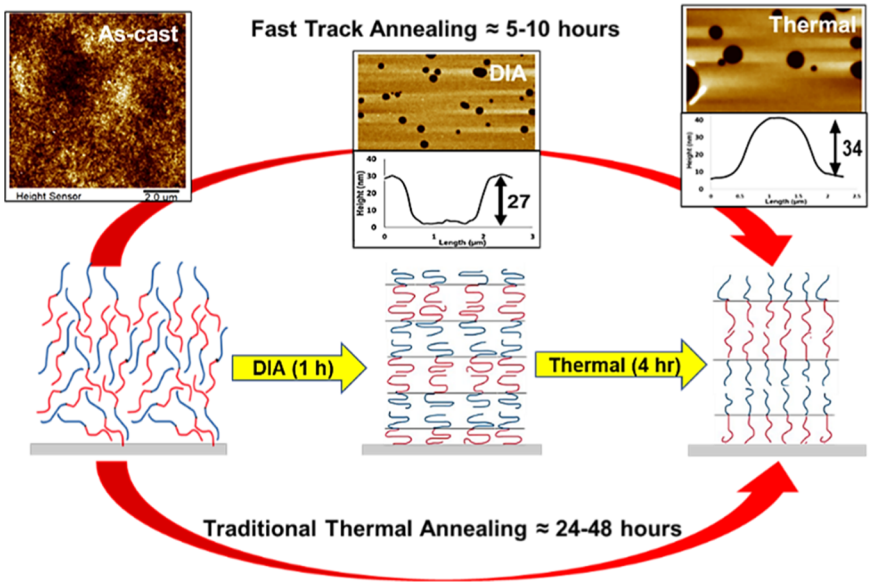

Figure 4. Fast-tracked annealing to achieve equilibrium large TA domain size by combined DIA and TA treatment. Numerical in the line height profiles are heights in nm.

ordered state compared to TA alone (Figure 4). Accelerated development of the thermal domain structure at high temperatures obscured the collection of detailed information on the transition mechanism. To slow down this transition, DIA-annealed films were thermally treated at lower temperatures of 160 °C (M_n = 36.5k and 51k) and 180 °C (M_n = 66k and 89k) in a vacuum for short durations. AFM height scans for these films revealed an undulating-surface transition morphology with large-height features, which can be seen in the line profiles in row 2 of Figure 2. Our experiments also showed that a pre-existing DIA morphology for low M_n (36.5k and 51k) BCPs accelerated the development of the subsequent thermal morphology even at low temperatures. The AFM scans in Figure S6; column 3 of the Supporting Information show that upon annealing DIA-treated low M_n BCPs of 36.5k and 51k at 160 °C in a vacuum, the morphology transformed into a well-developed TA morphology in about 1 h and 3 h, respectively. Island/hole topography did not fully develop for as-cast (disordered) films for the TA-only treatment at this temperature and time (Figure S6; column 2). For high M_n DIA-treated BCPs, 66k and 89k, sequential TA at 180 °C showed a transition to the multilayered island/hole morphology in 4 and 16 h, respectively. The same low-temperature TA-only treatment did not produce well-developed island/hole morphology from as-cast films (Figure S6; column 2). These results suggest that the sequential DIA + TA treatment can produce large domain size TA microstructures at lower temperatures than conventional TA, thus reducing the energy required for ordering. Besides using flow coating to cast films that uses the minimum amount of BCP solution, those coated using the conventional spin coating were also subjected to the same sequential annealing treatment. AFM topography analysis (Figures S7 and S8) showed that the spin-coated films of PS-*b*-PMMA with M_n = 51k and 66k have the same phase behavior compared to those cast via flow coating. So, the coating methodology does not influence the annealed microstructure.

DIA rapidly assembles the BCP film into a metastable lamellar structure, and a similar metastable structure was observed for SVA in a variety of solvents/solvent mixtures. In addition to using DIA as the first annealing step, films annealed via SVA in SM_1 were sequentially treated thermally at 160 °C for 51k and 180 °C for 66k in a vacuum. Both films displayed a transition to a multilayered island/hole morphology with larger TA domain sizes. Figure S5 also shows AFM height sensor scans for sequentially thermally annealed films. We find that even the initial SVA metastable microstructure can promote and expedite the development of larger TA lamellae.

To explore the degree of "metastable" order required using initial DIA processing that maximally expedites the subsequent thermal ordering transition, as-cast films of M_n = 66k were annealed with a relatively short DIA time followed by TA at a high temperature (180 °C) for only 2 h. The acquired AFM images are available in Figure S9 of the Supporting Information. The AFM analysis for this set reveals that merely 5 min of DIA treatment, wherein the island/hole morphology is only partially developed but has been reported previously to be sufficient time to initiate DIA assembly by Longanecker et al., was also sufficient to boost the transition to a higher domain size on subsequent TA. Not unexpectedly, the final morphology, in this case, was not very uniform and needed a longer thermal anneal. However, with an initial 10 to 20 min of DIA treatment, well-defined island/hole morphology with smaller domain sizes developed. Sequential TA then quickly produced the final melt-annealed microstructure within only 2 h. Notably, the final island/hole morphology produced was a three-step-multilayered domain structure, indicative of non-equilibrium pathway-dependent morphology. The formation of such a morphology suggests that further DIA time optimization is possible for even faster transitions to a fully developed TA microstructure via the sequential annealing (DIA/SVA + TA) technique.

To confirm that the domain height transitions observed using the AFM analysis occurred throughout the film thickness and were not just a surface phenomenon, NR was performed on DIA-equilibrated films and those annealed successively with TA for lamellar dPS-*b*-PMMA (M_n = 62k). The NR data fits and scattering length density (SLD) profiles, along with corresponding AFM height images for M_n = 66k treated under

https://doi.org/10.1021/acsami.2c21924
ACS Appl. Mater. Interfaces 2023, 15, 21562−21574

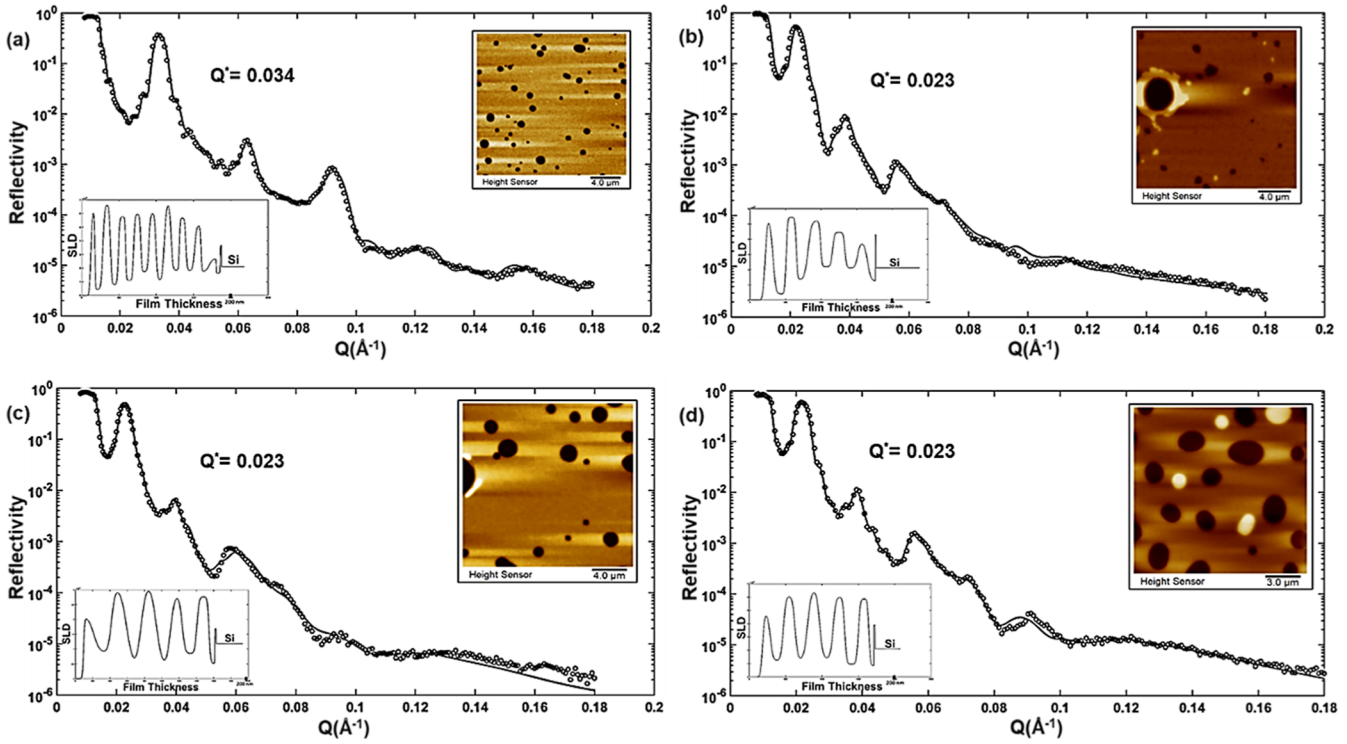

Figure 5. NR data (o) and fits (−) along with SLD profiles (inset-bottom left) for dPS-*b*-PMMA (M_n = 62k) films and corresponding AFM images for PS-*b*-PMMA (M_n = 66k) (inset-top right). (a) Films annealed via DIA in SM_1 for 1.5 h; (b) films annealed via DIA in SM_1 for 1.5 h followed by TA at 180 °C for 1 h; (c) films DIA annealed in SM_1 for 1.5 h followed by TA at 180 °C for 5 h; (d) films DIA annealed in SM_1 for 1.5 h followed by TA at 180 °C for 24 h. The values for Q^* in the inset are the positions of the Bragg peak ($L_o \sim Q^{*-1}$).

precisely the same conditions, are presented in Figure 5. The SLD after deuteration increases, and therefore the fitted profiles have higher SLD values where the density of dPS chains is higher, i.e., the dPS layers (SLD ≈ 6×10^{-6} Å^{-2}) compared to the PMMA layer (SLD ≈ 1×10^{-6} Å^{-2}). The SLD oscillations can be directly correlated to PS and PMMA layer variations along the film depth.

NR for as-cast films does not show a Bragg's peak (Figure S10). The SLD for the air-polymer interface is essentially zero, followed by a higher SLD layer confirming the presence of dPS on the film surface, owing to its lower surface energy. The NR samples were cast so that they have a commensurate/near-commensurate thickness to have a smooth surface for NR measurements. However, due to the large area of samples used, the induction of islands/holes topography cannot be completely eliminated. Further, due to a discrepancy in the domain sizes for TA and DIA, it is difficult to identify a thickness that is commensurate with respect to the periodicities of both structures. SLD values different than those for pure dPS and PMMA at the air interface are attributed to the presence of some island/hole topography on the film samples. The rightmost end of the SLD profile corresponds to a thin silicon oxide layer (SLD ≈ 3.4×10^{-6} Å^{-2}) followed by the Si substrate (SLD ≈ 2×10^{-6} Å^{-2}). The layer left to this silicon oxide layer has a low SLD due to the migration of the PMMA block.

The DIA-treated films displayed a well-defined SLD oscillation along the film depth with an average domain size of 25 nm. In just 1 h of thermal treatment, the Bragg peak in the reflectivity profile shifted to a lower Q value (formation of a larger L_o), and the SLD profile for the fitted NR data again displayed well-defined oscillations indicative of a periodic lamellar structure, with a larger average domain size of 35 nm. Further TA treatment only refined the microstructure and can be seen as improvements in the SLD profiles for films annealed for 5 h and 24 h. NR scans were also performed for intermediate TA times, and the fitted data is presented in Figure S11 to get a complete picture of the transient internal microstructure transition. NR thus confirmed the complete transition of the microstructure from DIA to the final melt-ordered state with faster kinetics compared to traditional TA alone.

DISCUSSION

Mechanism for Structural Rearrangement. The AFM and NR studies confirm the complete transition from DIA to TA microstructure, indistinguishable from that formed by long-time TA alone. DIA expedites BCP assembly due to high chain mobility and enhanced χ in the selective solvent-swollen state but leads to smaller domains for a parallel lamellar morphology. On the other hand, TA of lamellar BCP films creates large parallel domains from disorder ,but this process is slow owing to the relatively low mobility and reduced incompatibility (χ) in high temperature polymer melts. This microstructure transition study allowed us to explore chain rearrangement dynamics from a pre-existing structure and compare it to the arrangement dynamics from a disordered as-cast state. The current research in terms of molecular mass, treatment durations, and annealing conditions allows us to understand BCP order−order transitions and the parameters that affect them.

The transition from an as-cast to a DIA and thence to a TA lamellar microstructure is fast compared to the direct transition from the as-cast to the TA microstructure. From a disordered

https://doi.org/10.1021/acsami.2c21924
ACS Appl. Mater. Interfaces 2023, 15, 21562−21574

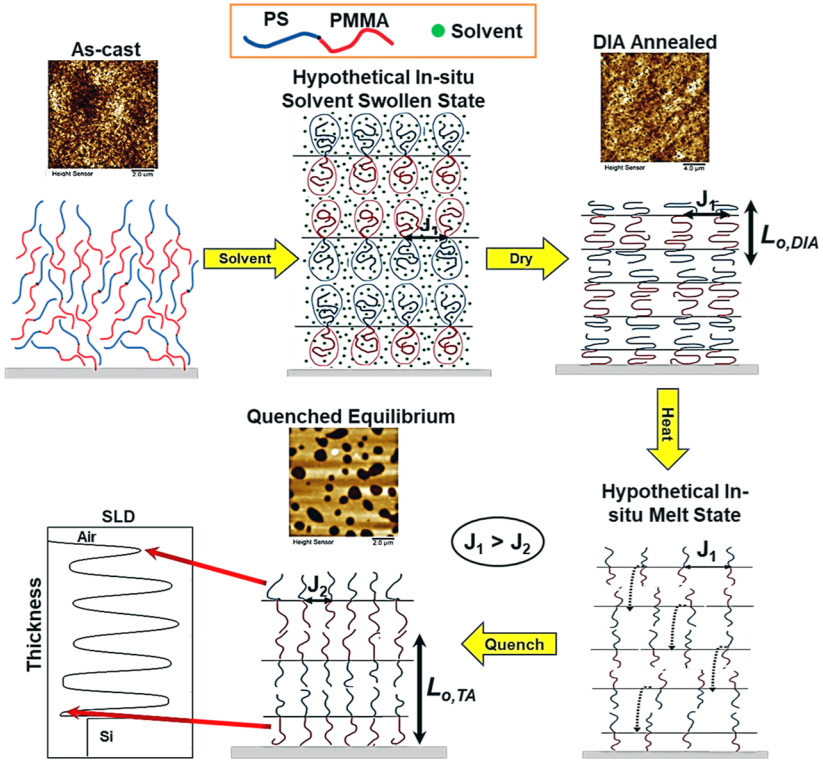

Figure 6. Proposed schematic for the transition from a DIA-annealed microstructure of collapsed chains to the thermally annealed microstructure. The chain junction spacing for the dried DIA morphology (J_1) is greater than that for the thermally annealed microstructure (J_2). The dotted arrows in Step 4 of the scheme show the proposed motion of relaxed polymer chains in the melt to rearrange into a lower number of layers with a higher domain size. The film thickness for the melt film is shown to be higher to account for the melt film expansion based on the coefficient of thermal expansion. The AFM height sensor images in the inset show the transition from a DIA-annealed morphology to a thermally annealed morphology for PS-*b*-PMMA (M_n = 66k) films.

state, the preferential segregation of PMMA to the Si substrate and the PS (lower surface energy) to the air interface marks the beginning of an ordering front. This ordering front then slowly moves toward the bulk of the film until it is entirely ordered.[46] Thin films show a stronger ordering drive from the substrate-segregated PMMA layer compared to the surface-segregated PS layer.[46] As molecular mass increases, despite a higher degree of segregation (higher χN) and thermodynamic driving force for lamellar ordering, the orienting forces for parallel lamellae decrease, producing a mixture of parallel and perpendicular orientations, especially in the middle portion of relatively thicker films.[47] For the sequential process, the diffusion rates in the melt are still low even when a pre-DIA-annealed film is subsequently annealed thermally. However, thermal ordering or rearrangement can now start from the pre-existing alternate layers of PS and PMMA of the DIA microstructure rather than partially segregated layers at the substrate-polymer and air-polymer interface in an as-cast film induced during the thermal or solvent casting process. Even the most rapidly formed DIA-induced structure creates weak but essential lamellar fluctuations that drastically lower the energy barrier for subsequent TA transition. We do not believe this dramatic lowering of the energy barrier to TA ordering by weakly (DIA in the present study, but alternatively by another method such as SVA) set-in lamellar fluctuations has until now been exploited in BCPs to achieve "fast-track" ordering. Furthermore, the formation of parallel ordering fronts throughout the film thickness may prevent mixed morphology defects from developing in the middle portion of thick films. We next showed (Figure S9) that having too high a degree of order locked in by the initial DIA process (at the wrong domain spacing compared to TA), in fact, makes it less efficient for subsequent TA-induced ordering. Thus, an optimal DIA time exists to obtain the fastest sequential ordering.

Importantly, the precursor DIA structure has a lower chain junction density due to collapsed layer structure with shrunk chains formed from a solvent-swollen state upon quick solvent evaporation. Upon sequential heating, these chains relax and stretch, and with the consequent larger junction spacing present, they can move more readily, enhancing the kinetics even further. These factors produce multiple ordering fronts that reassemble the film at an accelerated rate and create the multilayered island/hole surface morphology due to rearrangement at every interface. The schematic in Figure 6 describes the fast transition due to multiple ordering fronts. The DIA structure has a higher junction spacing J_1, which is retained in the post-DIA quenched film only until the film melts upon heating. In the melt, polymer chains move perpendicularly to the substrate, interchanging chains between every adjacent layer and quickly producing the thermally annealed structure of low junction spacing J_2, which is then quenched to room temperature.

Energetic Factors for Structural Rearrangement. The chain configurations in the DIA structure are of a collapsed nature, forming a greater number of thinner layers compared to the thicker and fewer layers obtained via TA. The energy associated with the greater number of layers for DIA can be studied through free energy models for confined BCPs. Turner approximated the free energy for a parallel lamellar BCP

https://doi.org/10.1021/acsami.2c21924
ACS Appl. Mater. Interfaces 2023, 15, 21562−21574

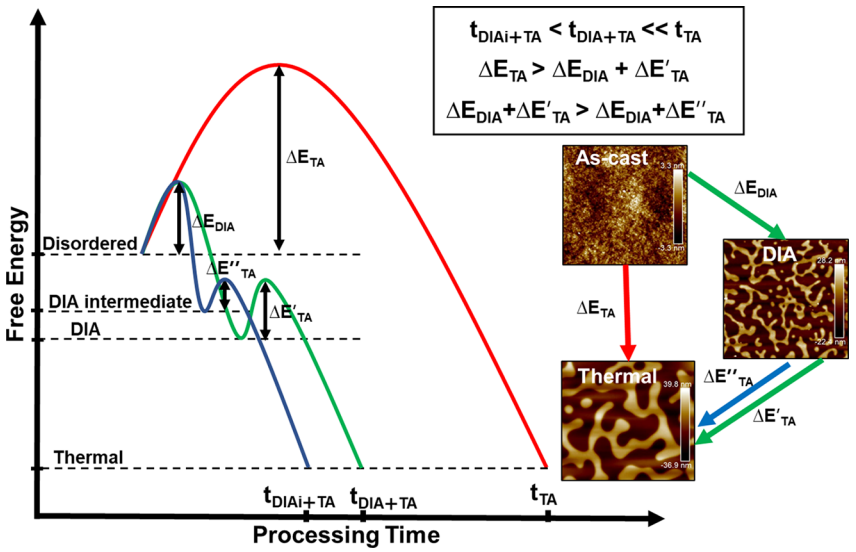

Figure 7. Schematic free energy diagram showing proposed energy states for as-cast disordered, DIA annealed, and thermally annealed BCP films. The energetic barrier for the direct TA process is higher than the combined energetic barrier for DIA+TA process. Note: There is an intermediate short-time DIA structure that can improve the transition kinetics further (blue line), and therefore, there is an optimal DIA ordered state (not too much nor too little order) that will result in the fastest sequential annealing time.

morphology for a polymer confined between parallel plates.[48] This treatment was extended by Walton et al. and can be expressed as[49]

$$\frac{F_h}{F_0} = \frac{1}{3}\left\{\lambda^2 + \frac{2}{\lambda} + \frac{1}{m\lambda}\left[\Gamma_1 + \Gamma_2 + \delta_k\left(\frac{1-(-1)^{2m}}{2}\right)\right]\right\} \quad (2)$$

where F_h is the free energy for the parallel morphology and F_0 is the bulk free energy. The parameter λ is the ratio of the lamellar period L obtained due to confinement with respect to the period L_o of the BCP in bulk, and Γ is the ratio of interfacial tensions (γ) for polymer-substrate and block−block interfaces (eq 3).[50,51]

$$\Gamma_1 = \frac{\gamma_{AS_1}}{\gamma_{AB}} \text{ and } \Gamma_2 = \frac{\gamma_{AS_2}}{\gamma_{AB}} \quad (3)$$

Here, A is the low surface energy block (PS here), B corresponds to PMMA, index 1 denotes the Si substrate, and index 2 is for air. δ is the ratio of the difference between the block-substrate interfacial tensions for a diblock relative to the block−block interfacial tensions (eq 4). The index k corresponds to the substrate near the high surface energy block, which in our case corresponds to PMMA,

$$\delta = \frac{\gamma_{BS} - \gamma_{AS}}{\gamma_{AB}} \quad (4)$$

The quantity L in the confined state will be lower than the natural period of the lamellar BCP due to the inhibition of island/hole formation by the confining surface. The value of $m = n$ (n = the number of lamellae) for symmetric wetting and $m = n + 0.5$ for asymmetric wetting of the substrate and air interfaces. If the same model can be applied to confinement in a thin film where one plate is the substrate while the other confinement is the boundary of the film (air-polymer interface), then for a specific BCP, all parameters are constant for both the morphologies obtained from DIA and TA except λ. The value of λ for DIA is much lower ($\lambda \approx 1/2$) compared to TA ($\lambda \approx 1$), which in turn attributes a higher free energy state to the DIA-annealed microstructure. Assuming the DIA domain size to be half of the thermal period, the number of interfaces between unlike polymers in DIA is always two per period more than that for TA. Calculating the interfacial area for the two morphologies for a film of constant volume assigns a greater interfacial area to the DIA-annealed structure and, in turn, greater interfacial energy. Modal calculations have been performed with experimental domain parameters using the described methods and are presented in the Supporting Information. A simple free energy diagram can be used to compare the energy states and transitions from disorder to order and order to order, as shown in Figure 7. Different morphologies with varying interfacial energies are assigned different energy levels, as shown by the dashed horizontal lines. The x-axis schematically plots the relative annealing times required for the sequential and TA-alone treatments. The disordered state with maximum contacts between unlike chains is assigned the highest energy. To achieve self-assembly via TA, the chains must overcome a significant barrier (ΔE_{TA}) due to low diffusion rates in the melt and poor incompatibility at high temperatures, especially for low χ BCPs like PS-b-PMMA. Due to slow diffusion, the initial segregation of PMMA to the substrate is slow and requires a long time for the initial layer to build up which can then direct further segregation into a layered structure. Overcoming this energy barrier of producing an initial segregated PMMA layer at the substrate and a PS layer at the air interface is reflected as the peak in free energy/required activation energy, and it takes a long time to achieve this state via conventional TA. On the other hand, DIA provides a pathway whereby the activation barrier is much lower due to higher diffusion rates in the solvent swollen state (low T_g) and increased incompatibility (high χ) due to preferential interaction between selective solvent components such as the solvent acetone and polar blocks like PMMA. On subsequent TA of the DIA structure, the barrier to rearrangement in the melt is much lower due to the availability of multiple ordering fronts at every DIA interface and the BCP system's inherent drive to reduce its interfacial energy/area

https://doi.org/10.1021/acsami.2c21924
ACS Appl. Mater. Interfaces 2023, 15, 21562−21574

(reduce the number of interfaces), despite the lower rate of diffusion. The secondary free energy peak/required activation energy for sequential annealing (DIA + TA) may be understood in terms of the extra interfaces created on chain rearrangement at every DIA interface, i.e., the multilayered terraces. A brief DIA immersion (<10 min) produces enough order/layering from the as-cast disordered state for sequential TA to achieve accelerated assembly with large domain sizes (Figure S9). In this case, the DIA microstructure resides at an intermediate energy level, and the degree of order is lower than that achieved at the local energy minimum of the metastable state, wherein the DIA island/hole surface morphology is fully developed. However, this limited degree of segregation is sufficient to drive assembly through multiple fronts upon TA, and the energy barrier becomes even smaller as the free surface of the film that did not have any island/holes post-short time-DIA does not require restructuring ($\Delta E_{TA}''$), shown as the blue curve in Figure 7. The reordering occurs at every DIA interface, producing a multi-terrace island/hole structure which resides at an intermediate level between DIA and disordered energy states. This mechanism that does not require film-free surface reorganization is reflected in Figure 7 as less TA time requirement from the DIA-ordered state to achieve the ground state. The complementary factors of DIA segregated layers and large chain junction spacings at the interface provide an alternate thermodynamic pathway to "fast-track" parallel lamellar morphologies with large TA domains, even for the high M_n BCPs studied. This route also exhibits a lower overall energy barrier when compared to the direct TA treatment.

CONCLUSIONS

Well-ordered BCP films featuring the traditional melt-annealed (TA) equilibrium domain (L_o) structure are obtained in a substantially shorter time by a cascade process that first involves immersion in a solvent mixture (DIA) or in solvent vapor (SVA) that forms a partially ordered metastable state, followed by TA that drives the structure to its global minimum. The sequential DIA + TA process is optimized when a DIA partially ordered state creates a minimally stratified ordered structure in a short time, albeit with a smaller domain spacing (e.g., $\approx L_o/2$) and large chain junction spacing, rather than a well-ordered structure with sharp interfaces at longer DIA process times. Evolution from this partially ordered BCP structure to its equilibrium L_o domain structure is achieved by subsequent TA for relatively short TA times. Thus, the overall processing time is much shorter compared to traditional melt annealing times from disordered BCP films. Our results demonstrate that in the thermal ordering of as-cast disordered BCP films, they must overcome a large energy barrier to construct the scaffold of a weakly ordered lamellar structure due to the relatively slow diffusion of BCP molecules in conjunction with wetting-driven parallel lamellar orientation only from the substrate and air interfaces. We utilize the high molecular mobility of DIA to circumvent the slow diffusive ordering barrier in TA to set up this lamellar scaffold for subsequent TA ordering. This work shows the potential of utilizing metastable local equilibrium structures as a transient pathway to arrive at a global equilibrium structure more efficiently, thereby bypassing high-energy barrier states that may be present in a single-step processing route. Herein, the sequential processing by DIA/SVA and TA provides a prospective route with a lower energy barrier to obtain parallel lamellar morphology, which is especially useful for ordering high molecular mass BCP films. More generally, solvation treatments for glassy polymer films can provide similar low-energy metastable transient routes for efficient processing to the desired final state.

MATERIALS AND METHODS

Experimental Design. Thin films of a diBCP were cast on silicon substrates and annealed in thermal, solvent mixture, and solvent vapor environments. The processing conditions (time, temperature, solvent mixtures, etc.) were chosen to identify an optimal sequential treatment to achieve accelerated BCP assembly.

Materials. Poly(styrene-*b*-methyl methacrylate) (PS-*b*-PMMA) diBCP was acquired from Polymer Source Inc. with an overall number average molecular mass of M_n = 20k (10k-*b*-10k), 36.5k (19.5k-*b*-17k), 51k (25k-*b*-26k), 66k (33k-*b*-33k), 89k (45k-*b*-44k), and 132k (65k-*b*-67k) g/mole. Deuterated poly(styrene-*b*-methyl methacrylate) (dPS-*b*-PMMA), where only the PS block was deuterated with M_n = 62k (32.5k-*b*-29.5k) g/mole, was also obtained from Polymer Source Inc. All block volume fractions correspond to a symmetric diblock (volume fraction of PS ≈ 0.5). BCP solutions were made in laboratory-grade toluene (VWR BDH Chemicals, ACS reagent, ≥99.5%) with a 30 to 50 mg/mL concentration (mass/vol). DIA and SVA were performed in sealed glass jars. DIA/SVA solvent mixtures are composed of heptane (VWR BDH Chemicals, Laboratory reagent, ≥99.9%), acetone (VWR BDH Chemicals, ACS reagent, ≥99.5%), toluene (VWR BDH Chemicals, ACS reagent, ≥99.5%), and tetrahydrofuran (THF—Macron Fine Chemicals, ACS reagent, ≥99.0%).

BCP Thin-Film Preparation. Thin films were cast from solutions of PS-*b*-PMMA of different molecular masses and dPS-*b*-PMMA in toluene using the flow coating method. This method requires only minute quantities of the polymer solution. The polymer solution was pipetted into the gap between an angled glass blade and a flat Si substrate (substrate UVO treated for 120 min). The blade edge moved along the substrate, pulling the solution along and coating a layer onto the substrate. Films were also prepared using the standard spin coating method to confirm the effects of the film coating technique on the sequential treatment.

Annealing Treatments. DIA was done in sealed glass jars at room temperature (≈25 °C). The solvent mixture was composed of heptane, acetone, and toluene in the solvent mixture (SM) proportions of SM_0 = 80:15:5, SM_1 = 75:25:5, and SM_2 = 60:30:10 by volume, respectively. The composition SM_1 has been reported to be optimum for low M_n lamellar PS-*b*-PMMA by Longanecker et al. The concentrations of the good solvents were increased or decreased with respect to SM_1 to expedite assembly for high M_n BCP films or to prevent dewetting of low M_n BCP films. Here, heptane is a non-solvent for both PS and PMMA, toluene is a neutral good solvent for both, and acetone is a selective good solvent for PMMA. DIA immersion times were also varied with the BCP molecular mass for any particular SM. All films were heated on a hot plate at 60 °C for 5 to 10 min to remove any residual solvent post-DIA. A set of films was also vacuum (≈100 kPa) dried at 80 °C for 24 h to study the effect of residual solvent on the sequential TA.

SVA was done in sealed glass jars at room temperature (≈25 °C). The jar volume is ≈70 mL, and the solvent bath volume is ≈5 mL. The films were placed on a stage ≈1 cm above the solvent bath surface. Annealing times varied from a few minutes up to a few hours. The solvents studied include acetone, THF, and the solvent mixture 1, also used for DIA of intermediate M_n BCPs. Films were dried on a hot stage at 60 °C for 5 to 10 min.

TA was performed in vacuum ovens at ≈100 kPa vacuum at temperatures ranging from 160 to 200 °C. All samples were quenched to room temperature (≈25 °C) post-TA.

Characterization. Film thicknesses were measured using UV interferometry on the Filmetrics LS-DT2 interferometer. The topography of the polymer−air interface for thin films was characterized using a Bruker AXS Dimension Icon AFM in standard tapping mode in air. Height sensor and phase scans were obtained for

https://doi.org/10.1021/acsami.2c21924
ACS Appl. Mater. Interfaces 2023, 15, 21562−21574

all film samples. NR was performed to analyze the internal film microstructure on the NG7 horizontal neutron reflectometer, available at the NIST Center for Neutron Research. The instrument has an incident neutron wavelength of 4.77 Å, a wavelength range of 2.3−5.5 Å, and an available Q range of 0.003 to 0.24 $Å^{-1}$. Film samples used for NR had a deuterated PS block. NR measures film thickness from the periodicity of the fringe oscillations and film local SLD as a function of film depth (thus deuterated PS layers are clearly distinguished from non-deuterated PMMA layers) when fitted with a model that incorporates these parameters. Technically, the acquired data was reduced using "ReflRed software" and analyzed using the "REFLPAK" package developed by NIST that fits the reflectivity data to a layer model of the sample. This is a forward-fitting method that allows one to manually manipulate parameters like domain spacing, interfacial width, layer SLD, etc., to fit the NR data. The automatic fit method does a gradient descent search through the selected fitting parameter space using a Levenberg−Marquardt non-linear least squares update procedure. Each iteration updates the parameter table, and at the end of the fit, it estimates the uncertainty in each parameter. Some NR experiments were performed on the LIQREF reflectometer at Oak Ridge National Laboratory to confirm internal morphologies for films successively treated for intermediate annealing times. The instrument also measures in horizontal sample geometry, has a wavelength range of 2.5−17 Å, and an available Q range of 0.008−0.3 $Å^{-1}$.

■ ASSOCIATED CONTENT

Supporting Information

The Supporting Information is available free of charge at https://pubs.acs.org/doi/10.1021/acsami.2c21924.

AFM images and NR profiles for films annealed from as-cast to DIA, as-cast to TA, and DIA to TA; comparative AFM study for SVA-treated PS-*b*-PMMA films and sequential SVA + TA-treated films with respect to DIA and DIA + TA-treated BCP films; and model-free energy calculations for TA and DIA microstructures (PDF)

■ AUTHOR INFORMATION

Corresponding Authors

Jack F. Douglas − *Materials Science and Engineering Division, National Institute of Standards and Technology, Gaithersburg, Maryland 20899, United States;* orcid.org/0000-0001-7290-2300; Email: jack.douglas@nist.gov

Alamgir Karim − *William A. Brookshire, Department of Chemical & Biomolecular Engineering, University of Houston, Houston, Texas 77204, United States;* orcid.org/0000-0003-1302-9374; Email: akarim3@central.uh.edu

Authors

Kshitij Sharma − *William A. Brookshire, Department of Chemical & Biomolecular Engineering, University of Houston, Houston, Texas 77204, United States;* orcid.org/0000-0001-7309-5352

Aman Agrawal − *William A. Brookshire, Department of Chemical & Biomolecular Engineering, University of Houston, Houston, Texas 77204, United States*

Ali Masud − *William A. Brookshire, Department of Chemical & Biomolecular Engineering, University of Houston, Houston, Texas 77204, United States*

Sushil K. Satija − *National Institute of Standards and Technology, Center for Neutron Research, Gaithersburg, Maryland 20899, United States*

John F. Ankner − *Second Target Station Project, Oak Ridge National Laboratory, Oak Ridge, Tennessee 37830, United States;* orcid.org/0000-0002-6737-5718

Complete contact information is available at: https://pubs.acs.org/10.1021/acsami.2c21924

Funding

We acknowledge NSF DMR 1905996 for support of the research.

Notes

Certain commercial materials and equipment are identified to specify adequately the experimental procedure. In no case does such identification imply recommendation by the National Institute of Standards and Technology, nor does it imply that the material or equipment identified is necessarily the best available for this purpose.

The authors declare no competing financial interest.

■ REFERENCES

(1) Bates, F. S.; Fredrickson, G. H. Block Copolymer Thermodynamics : Theory and Experiment. *Annu. Rev. Phys. Chem.* **1990**, *41*, 525−557.

(2) Bates, F. S.; Fredrickson, G. H. Block Copolymers-Designer Soft Materials. *Phys. Today* **1999**, *52*, 32−38.

(3) Zhang, C. Z.; Wang, Z. G. Random Isotropic Structures and Possible Glass Transitions in Diblock Copolymer melts. *Phys. Rev. E: Stat., Nonlinear, Soft Matter Phys.* **2006**, *73*, 031804.

(4) Müller, M.; Sun, D. W. Directing the Self-assembly of Block Copolymers into a Metastable Complex Network Phase via a Deep and Rapid Quench. *Phys. Rev. Lett.* **2013**, *111*, 267801.

(5) Kim, K.; Schulze, M. W.; Arora, A.; Lewis, R. M.; Hillmyer, M. A.; Dorfman, K. D.; Bates, F. S. Thermal Processing of Diblock Copolymer Melts Mimics Metallurgy. *Science* **2017**, *356*, 520−523.

(6) Bosse, A. W.; Douglas, J. F.; Berry, B. C.; Jones, R. L.; Karim, A. Block-copolymer Ordering with a Spatiotemporally Heterogeneous Mobility. *Phys. Rev. Lett.* **2007**, *99*, 216101.

(7) Menelle, A.; Russell, T. P.; Anastasiadis, S. H.; Satija, S. K.; Majkrzak, C. F. Ordering of Thin Diblock Copolymer Films. *Phys. Rev. Lett.* **1992**, *68*, 67−70.

(8) Russell, T. P.; Menelle, A.; Anastasiadis, S. H.; Satija, S. K.; Majkrzak, C. F. Ordering of Thin Films of Symmetric Diblock Copolymers. *Prog. Colloid Polym. Sci.* **1993**, *91*, 97−100.

(9) Mutter, R.; Stuehn, B. Static and Kinetic Aspects of the Ordering Transition in Thin Films of Diblock Copolymers. *Macromolecules* **1995**, *28*, 5022−5028.

(10) Smith, A. P.; Douglas, J. F.; Meredith, J. C.; Amis, E. J.; Karim, A. Combinatorial Study of Surface Pattern Formation in Thin Block Copolymer Films. *Phys. Rev. Lett.* **2001**, *87*, 015503.

(11) Smith, A. P.; Douglas, J. F.; Meredith, J. C.; Amis, E. J.; Karim, A. High-throughput Characterization of Pattern Formation in Symmetric Diblock Copolymer Films. *J. Polym. Sci., Part B: Polym. Phys.* **2001**, *39*, 2141−2158.

(12) Smith, A. P.; Douglas, J. F.; Amis, E. J.; Karim, A. Effect of Temperature on the Morphology and Kinetics of Surface Pattern Formation in Thin Block Copolymer Films. *Langmuir* **2007**, *23*, 12380−12387.

(13) Coulon, G.; Russell, T. P.; Deline, V. R.; Green, P. F. Surface-Induced Orientation of Symmetric, Diblock Copolymers: A Secondary Ion Mass Spectrometry Study. *Macromolecules* **1989**, *22*, 2581−2589.

(14) Zhao, Y.; Hashimoto, T.; Douglas, J. F. Frustrating the Lamellar Ordering Transition of Polystyrene-block- polyisoprene with a C60 Additive. *J. Chem. Phys.* **2009**, *130*, 124901.

(15) Barnes, K. A.; Karim, A.; Douglas, J. F.; Nakatani, A. I.; Gruell, H.; Amis, E. J. Suppression of Dewetting in Nanoparticle-filled Polymer Films. *Macromolecules* **2000**, *33*, 4177−4185.

(16) Kubo, M.; Takahashi, Y.; Fujii, T.; Liu, Y.; Sugioka, K. i.; Tsukada, T.; Minami, K.; Adschiri, T. Thermal Dewetting Behavior of Polystyrene Composite Thin Films with Organic-modified Inorganic Nanoparticles. *Langmuir* **2014**, *30*, 8956−8964.
(17) Mukherjee, R.; Das, S.; Das, A.; Sharma, S. K.; Raychaudhuri, A. K.; Sharma, A. Stability and Dewetting of Metal Nanoparticle Filled Thin Polymer Films: Control of Instability Length Scale and Dynamics. *ACS Nano* **2010**, *4*, 3709−3724.
(18) Samant, S. P.; Grabowski, C. A.; Kisslinger, K.; Yager, K. G.; Yuan, G.; Satija, S. K.; Durstock, M. F.; Raghavan, D.; Karim, A. Directed Self-Assembly of Block Copolymers for High Breakdown Strength Polymer Film Capacitors. *ACS Appl. Mater. Interfaces* **2016**, *8*, 7966−7976.
(19) Samant, S.; Basutkar, M.; Singh, M.; Masud, A.; Grabowski, C. A.; Kisslinger, K.; Strzalka, J.; Yuan, G.; Satija, S.; Apata, I.; et al. Effect of Molecular Weight and Layer Thickness on the Dielectric Breakdown Strength of Neat and Homopolymer Swollen Lamellar Block Copolymer Films. *ACS Appl. Polym. Mater.* **2020**, *2*, 3072−3083.
(20) Modi, A.; Bhaway, S. M.; Vogt, B. D.; Douglas, J. F.; Al-Enizi, A.; Elzatahry, A.; Sharma, A.; Karim, A. Direct Immersion Annealing of Thin Block Copolymer Films. *ACS Appl. Mater. Interfaces* **2015**, *7*, 21639−21645.
(21) Longanecker, M.; Modi, A.; Dobrynin, A.; Kim, S.; Yuan, G.; Jones, R.; Satija, S.; Bang, J.; Karim, A. Reduced Domain size and Interfacial Width in Fast Ordering Nanofilled Block Copolymer Films by Direct Immersion Annealing. *Macromolecules* **2016**, *49*, 8563−8571.
(22) Ruiz, R.; Bosworth, J. K.; Black, C. T. Effect of Structural Anisotropy on the Coarsening Kinetics of Diblock Copolymer Striped Patterns. *Phys. Rev. B* **2008**, *77*, 054204.
(23) Berry, B. C.; Bosse, A. W.; Douglas, J. F.; Jones, R. L.; Karim, A. Orientational Order in Block Copolymer Films Zone Annealed below the Order − Disorder Transition Temperature. *Nano Lett.* **2007**, *7*, 2789−2794.
(24) Majewski, P. W.; Yager, K. G. Millisecond Ordering of Block Copolymer Films *via* Photothermal Gradients. *ACS Nano* **2015**, *9*, 3896−3906.
(25) Wu, W.; Singh, M.; Masud, A.; Wang, X.; Nallapaneni, A.; Xiao, Z.; Zhai, Y.; Wang, Z.; Terlier, T.; Bleuel, M.; et al. Control of Phase Morphology of Binary Polymer Grafted Nanoparticle Blend Films via Direct Immersion Annealing. *ACS Nano* **2021**, *15*, 12042−12056.
(26) Zeman, L.; Patterson, D. Effect of the Solvent on Polymer Incompatibility in Solution. *Macromolecules* **1972**, *5*, 513−516.
(27) Sinturel, C.; Vayer, M.; Morris, M.; Hillmyer, M. A. Solvent Vapor Annealing of Block Polymer Thin Films. *Macromolecules* **2013**, *46*, 5399−5415.
(28) Alagbe, B. D.; Gibb, B. C.; Ashbaugh, H. S. Evolution of the Free Energy Landscapes ofn-Alkane Guests Bound within Supramolecular Complexes. *J. Phys. Chem. B* **2021**, *125*, 7299−7310.
(29) Kearns, K. L.; Swallen, S. F.; Ediger, M. D.; Wu, T.; Sun, Y.; Yu, L. Hiking Down the Energy Landscape: Progress Toward the Kauzmann Temperature via Vapor Deposition. *J. Phys. Chem. B* **2008**, *112*, 4934−4942.
(30) Ediger, M. D. Perspective: Highly Stable Vapor-deposited Glasses. *J. Chem. Phys.* **2017**, *147*, 210901.
(31) Singh, G.; Yager, K. G.; Berry, B.; Kim, H.; Karim, A. Dynamic Thermal Field-Induced Gradient Soft-Shear for Highly Oriented Block Copolymer Thin Films. *ACS Nano* **2012**, *6*, 10335−10342.
(32) Chung, S. Y.; Kim, Y. M.; Kim, J. G.; Kim, Y. J. Multiphase Transformation and Ostwalds Rule of Stages during Crystallization of a Metal Phosphate. *Nat. Phys.* **2009**, *5*, 68−73.
(33) Washington, A. L.; Foley, M. E.; Cheong, S.; Quffa, L.; Breshike, C. J.; Watt, J.; Tilley, R. D.; Strouse, G. F. Ostwald's Rule of Stages and its Role in CdSe Quantum Dot Crystallization. *J. Am. Chem. Soc.* **2012**, *134*, 17046−17052.
(34) Ungar, G.; Stejny, J.; Keller, A.; Bidd, I.; Whiting, M. C. The Crystallization of Ultralong Normal Paraffins: The Onset of Chain Folding. *Science* **1985**, *229*, 386−389.
(35) Higgs, P. G.; Ungar, G. The Growth of Polymer Crystals at the Transition from Extended Chains to Folded Chains. *J. Chem. Phys.* **1994**, *100*, 640−648.
(36) Gotrik, K. W.; Ross, C. A. Solvothermal Annealing of Block Copolymer Thin Films. *Nano Lett.* **2013**, *13*, 5117−5122.
(37) Zhang, X.; Harris, K. D.; Wu, N. L. Y.; Murphy, J. N.; Buriak, J. M. Fast Assembly of Ordered Block Copolymer Nanostructures through Microwave Annealing. *ACS Nano* **2010**, *4*, 7021−7029.
(38) Cummins, C.; Mokarian-tabari, P.; Andreazza, P.; Sinturel, C.; Morris, M. A. Solvothermal Vapor Annealing of Lamellar Poly(styrene)-*block*-poly(d,l-lactide) Block Copolymer Thin Films for Directed Self-Assembly Application. *ACS Appl. Mater. Interfaces* **2016**, *8*, 8295−8304.
(39) Shi, L. Y.; Lan, J.; Lee, S.; Cheng, L. C.; Yager, K. G.; Ross, C. A. Vertical Lamellae Formed by Two-Step Annealing of a Rod-Coil Liquid Crystalline Block Copolymer Thin Film. *ACS Nano* **2020**, *14*, 4289−4297.
(40) Stasiak, P.; McGraw, J. D.; Dalnoki-Veress, K.; Matsen, M. W. Step Edges in Thin Films of Lamellar-forming Diblock Copolymer. *Macromolecules* **2012**, *45*, 9531−9538.
(41) Maher, M. J.; Self, J. L.; Stasiak, P.; Blachut, G.; Ellison, C. J.; Matsen, M. W.; Bates, C. M.; Willson, C. G. Structure, Stability, and Reorganization of 0.5 L0 Topography in Block Copolymer Thin Films. *ACS Nano* **2016**, *10*, 10152−10160.
(42) Masud, A.; Longanecker, M.; Bhadauriya, S.; Singh, M.; Wu, W.; Sharma, K.; Terlier, T.; Al-Enizi, A. M.; Satija, S.; Douglas, J. F.; et al. Ionic Liquid Enhanced Parallel Lamellar Ordering in Block Copolymer Films. *Macromolecules* **2021**, *54*, 4531−4545.
(43) Ahn, H.; Ryu, D. Y.; Kim, Y.; Kwon, K. W.; Lee, J.; Cho, J. Phase Behavior of Polystyrene-b-poly(methyl methacrylate) Diblock Copolymer. *Macromolecules* **2009**, *42*, 7897−7902.
(44) Masud, A.; Wu, W.; Singh, M.; Tonny, W.; Ammar, A.; Sharma, K.; Strzalka, J. W.; Terlier, T.; Douglas, J. F.; Karim, A. Solvent Processing and Ionic Liquid-Enabled Long-Range Vertical Ordering in Block Copolymer Films with Enhanced Film Stability. *Macromolecules* **2021**, *54*, 8512−8525.
(45) Anastasiadis, S. H.; Russell, T. P.; Satija, S. K.; Majkrzak, C. F. The Morphology of Symmetric Diblock Copolymers as Revealed by Neutron Reflectivity. *J. Chem. Phys.* **1990**, *92*, 5677−5691.
(46) Russell, T. P.; Coulon, G.; Deline, V. R.; Miller, D. C. Characteristics of the Surface-Induced Orientation for Symmetric Diblock PS/PMMA Copolymers. *Macromolecules* **1989**, *22*, 4600−4606.
(47) Huang, E.; Mansky, P.; Russell, T. P.; Harrison, C.; Chaikin, P. M.; Register, R. A.; Hawker, C. J.; Mays, J. Mixed Lamellar Films: Evolution, Commensurability Effects, and Preferential Defect Formation. *Macromolecules* **2000**, *33*, 80−88.
(48) Turner, M. S. Equilibrium Properties of a Diblock Copolymer Lamellar Phase Confined between Flat Plates. *Phys. Rev. Lett.* **1992**, *69*, 1788−1791.
(49) Walton, D. G.; Kellogg, G. J.; Mayes, A. M.; Lambooy, P.; Russell, T. P. A Free Energy Model for Confined Diblock Copolymers. *Macromolecules* **1994**, *27*, 6225−6228.
(50) Wu, S. Calculation of Interfacial Tension in Polymer Systems. *J. Polym. Sci., Part C: Polym. Symp.* **2007**, *34*, 19−30.
(51) Mortezaei, M.; Famili, M. H. N.; Kokabi, M. The Role of Interfacial Interactions on the Glass-transition and Viscoelastic Properties of Silica/Polystyrene Nanocomposite. *Compos. Sci. Technol.* **2011**, *71*, 1039−1045.

https://doi.org/10.1021/acsami.2c21924
ACS Appl. Mater. Interfaces 2023, 15, 21562−21574